

## Supplementary Information:

### Single-atom vs Single-Superatom as Catalysts for Ammonia Production

Mehmet Emin Kilic and Puru Jena\*

Physics Department, Virginia Commonwealth University, Richmond, VA 23284

#### Abstract

##### Theoretical Methods:

All geometry optimizations are performed using the spin-polarized DFT method implemented in the Vienna ab initio Simulation Package (VASP)<sup>1,2</sup> and Gaussian 16<sup>3</sup>. The projector augmented wave (PAW) method<sup>4</sup> is utilized to address electron-ion interactions, with a plane wave energy cutoff set at 520 eV. The exchange correlation potential is calculated using the generalized gradient approximation (GGA) and the Perdew–Burke–Ernzerhof (PBE) functional<sup>5</sup>. A 6x6x1 gamma-centered k-points sampling a Brillouin zone are set in all the structure relaxations. The Grimme DFT-D3 algorithm is used to correct for van der Waals interactions<sup>6</sup>. The convergence criteria of energy and Hellman-Feynman forces on each atom are set as  $10^{-5}$  eV and  $10^{-2}$  eV/Å, respectively. The vacuum space is set at least 15 Å, which is large enough to guarantee a sufficient separation between periodic images.

To determine the minimum energy paths (MEP), we performed the transition state calculations using the nudged elastic band (NEB) method<sup>7</sup>. This method optimizes a chain of images linking the initial state (IS) and the final state (FS). Each image is constrained to move only in the direction perpendicular to the tangent of the path. Thus, the energy is minimized in all directions except along the reaction path.

The stability of the catalysts is evaluated by performing the ab-initio molecular dynamics (AIMD) simulations in the NVT ensemble using the Nose-Hoover thermostat. We initialized our AIMD simulations from a fully relaxed structure obtained through DFT calculations at 0 K. During the simulations, we closely monitored the potential energy of the system, as it is sensitive to bond breaking and formations. After 0.5 ps, the energy remained nearly constant, with only small fluctuations due to thermal vibrations, which indicates that the system had reached a steady state. Therefore, we confirm that the system was adequately pre-equilibrated, and all trajectory analyses were reported after this equilibration phase.

The computational hydrogen electrode model (CHE) is used for the proton-electron transfer step where the half of the chemical potential of H<sub>2</sub> is equal to the chemical potential of the proton/electron (H<sup>+</sup>/e<sup>-</sup>) pair under standard conditions [pH=0, U=0V, p(H<sub>2</sub>) = 1 atm]<sup>8,9</sup>. The free energy change ( $\Delta G$ ) of each H<sup>+</sup>/e<sup>-</sup> step is described as:

$$\Delta G = \Delta E + \Delta E_{\text{ZPE}} - T\Delta S + \Delta G_U, \quad (1)$$

where  $\Delta E$  is the electronic energy obtained from DFT,  $\Delta E_{\text{ZPE}}$  is the change in zero-point energy

calculated from  $E_{\text{ZPE}} = \frac{1}{2} \sum_{i=1}^N h\nu_i$  where N is the number of vibration modes. T is the temperature (298.15 K) and  $\Delta S$  is the change in entropy. The entropies of the gas phase are taken from the NIST database.  $\Delta G_U$  is obtained from  $\Delta G_U = -eU$  where  $e$  represents the transferred charge, and  $U$  represents the potential on the electrode. According to the computational electrode catalyst, the thermodynamic energy barrier is equal to the maximum free energy difference, or the reaction potential determining step (PDS).

The binding energy of  $X$  (where  $X$  represents a single-atom, super-atom, or molecule) on the  $Y$  surface is calculated using the expression:  $E_B = E_{XY} - E_X - E_Y$ , where  $E_{XY}$  is the total energy of the system consisting of  $X$  and  $Y$ , and  $E_X$  and  $E_Y$  are the total energies of the isolated  $X$  and  $Y$ , respectively.

**Table S1.** Calculated ionization potential (IP) in eV, electron affinity (EA) in eV, equilibrium bond distance in Å, and vibrational frequency (cm<sup>-1</sup>) of isolated N<sub>2</sub> molecule using different basis set and B3LYP functional<sup>10-12</sup>.

Basis sets	IP (eV)	EA (eV)	$d(\text{N}\equiv\text{N})$ (Å)	Frequency (cm <sup>-1</sup> )
631G	15.83	-1.54	1.105	2454
6311G	15.87	-1.61	1.096	
aug-cc-pVDZ	15.81	-1.53	1.104	
aug-cc-pVTZ	15.84	-1.59	1.091	
cc-pVDZ	15.62	-2.81	1.104	
cc-pVTZ	15.79	-2.31	1.091	
def2-TZVP	15.82	-2.03	1.091	2453

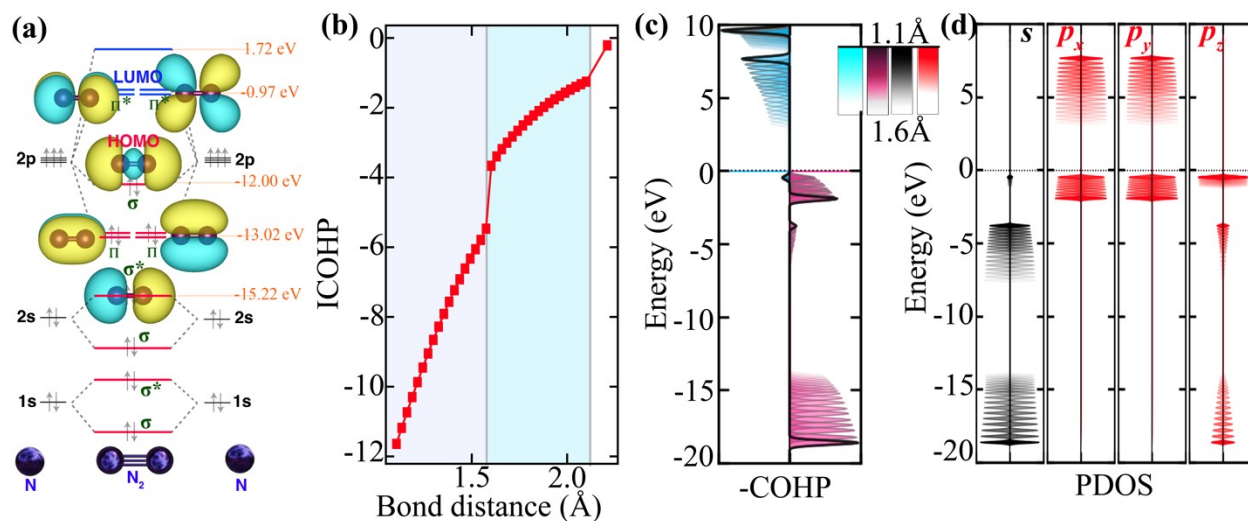


**Fig. S1** (a) MO diagram of the N<sub>2</sub> molecule. (b) Variation in ICOHP value as a function of bond distance. (c) Variation in COHP as a function of bond distance, shown for ranges between 1.1 to 1.6 Å, with antibonding states in cyan and bonding states in pink. (d) PDOS as a function of bond distance, with ranges of 1.1 to 1.6 Å, where *s* and *p* (*p<sub>x</sub>*, *p<sub>y</sub>*, and *p<sub>z</sub>*) orbitals are depicted in black and red, respectively.

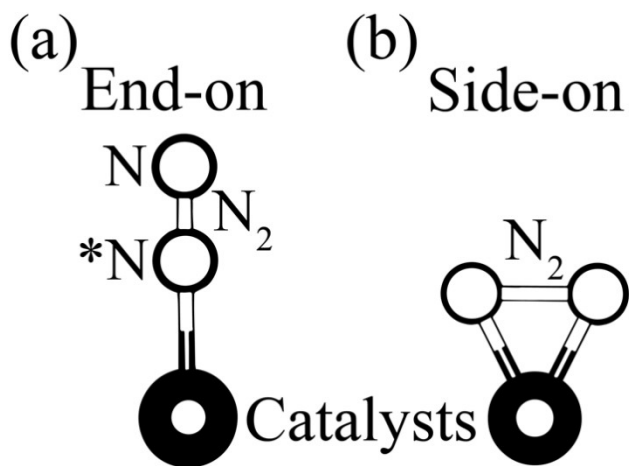


**Fig. S2.** Two typical adsorption configurations for N<sub>2</sub> molecule: (a) end-on and (b) side-on.

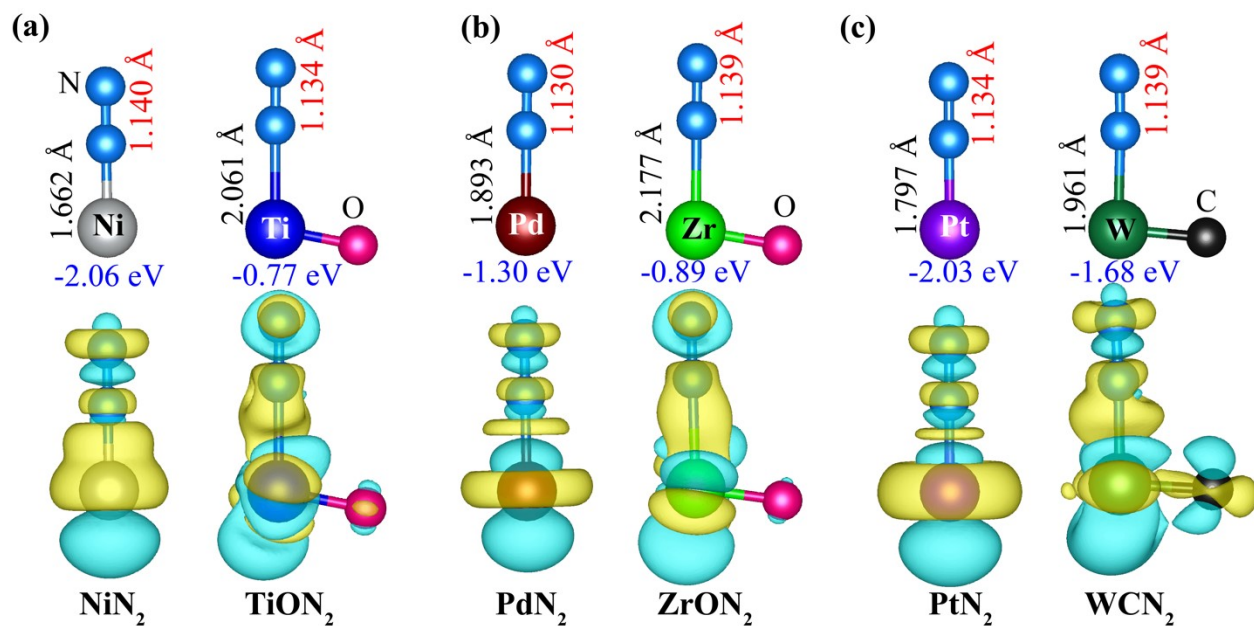


**Fig. S3** Upper panel: Equilibrium atomic configurations for the adsorption of N<sub>2</sub> on single (super)-atoms of Ni (TiO), Pd (ZrO), and Pt (WC) in the gas phase. Lower panel: Charge density difference where yellow and cyan regions represent charge accumulations and depletions, respectively.

**Table S2.** Charge transfer to the adsorbed N<sub>2</sub> molecule ( $\Delta q$ , in e), the N≡N bond distance ( $d_{\text{NN}}$ , in Å), and the binding energy ( $E_{\text{B}}$ , in eV) for N<sub>2</sub> adsorption on Ni (TiO), Pd (ZrO), and Pt (WC) with and without a graphene substrate

	Isolated single- and super-atoms			Single- and super-atoms supported on graphene		
	Ni (TiO)	Pd (ZrO)	Pt (WC)	Ni (TiO)	Pd (ZrO)	Pt (WC)
$\Delta q$	0.29 (0.27)	0.20 (0.36)	0.15 0.26	0.28 (0.26)	0.20 (0.34)	0.22 (0.34)
$d_{\text{NN}}$	1.140 (1.134)	1.130 (1.139)	1.135 (1.140)	1.135 (1.132)	1.128 (1.137)	1.132 (1.140)
$E_{\text{B}}$	-2.06	-1.30	-2.03	-1.94	-1.20	-1.88

	(-0.77)	(-0.89)	(-1.68)	-0.85	-1.00	-1.74
--	---------	---------	---------	-------	-------	-------

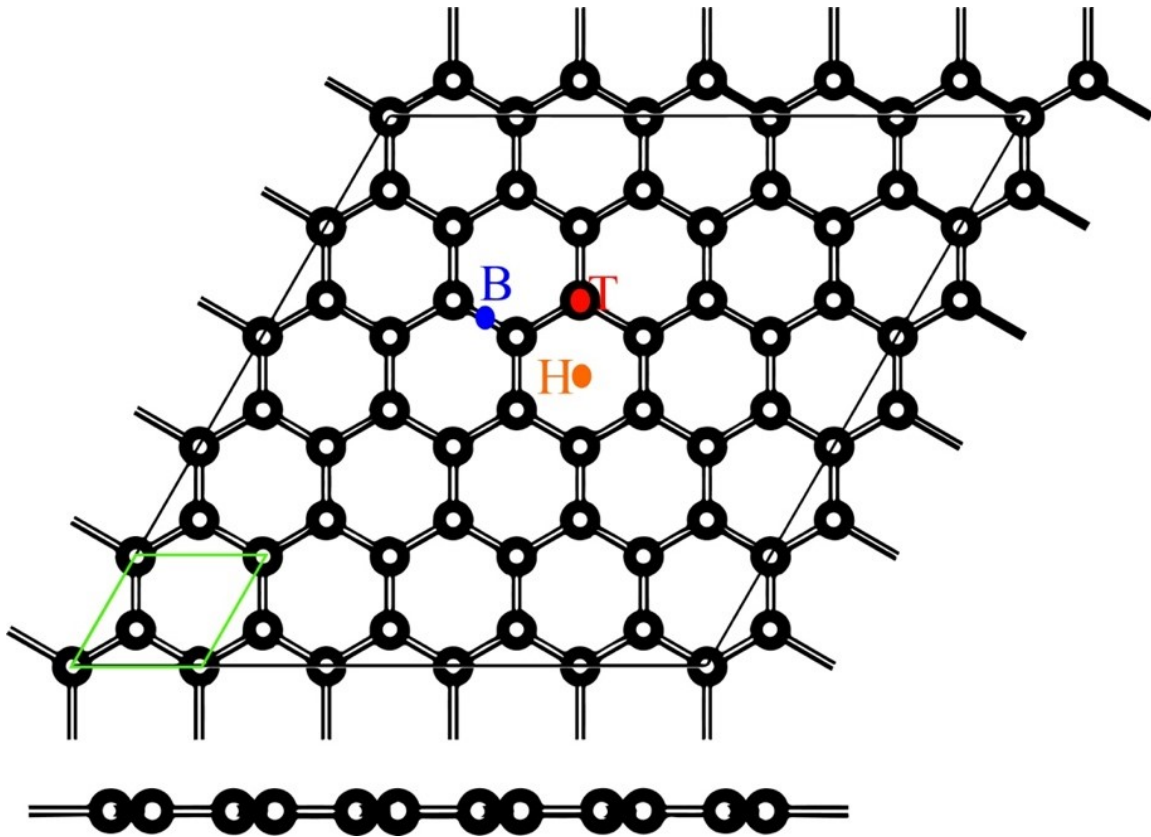


**Fig. S4.** A 5x5x1 supercell of graphene, with the bridge, hollow, and top symmetric sites denoted as B, H, and T, respectively. The unit-cell of graphene is framed in green.

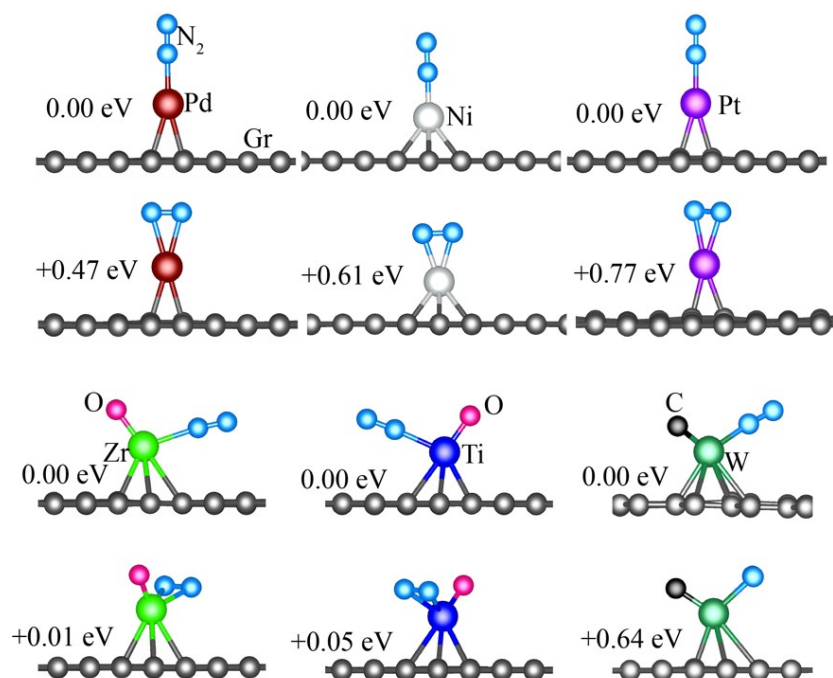


**Fig. S5** Optimized atomic configuration of N<sub>2</sub> adsorbed on Pd (ZrO), Ni (TiO), Pt (WC) supported on graphene with side-on and end-on configuration where the total energy of end-on configuration is set to 0 eV.

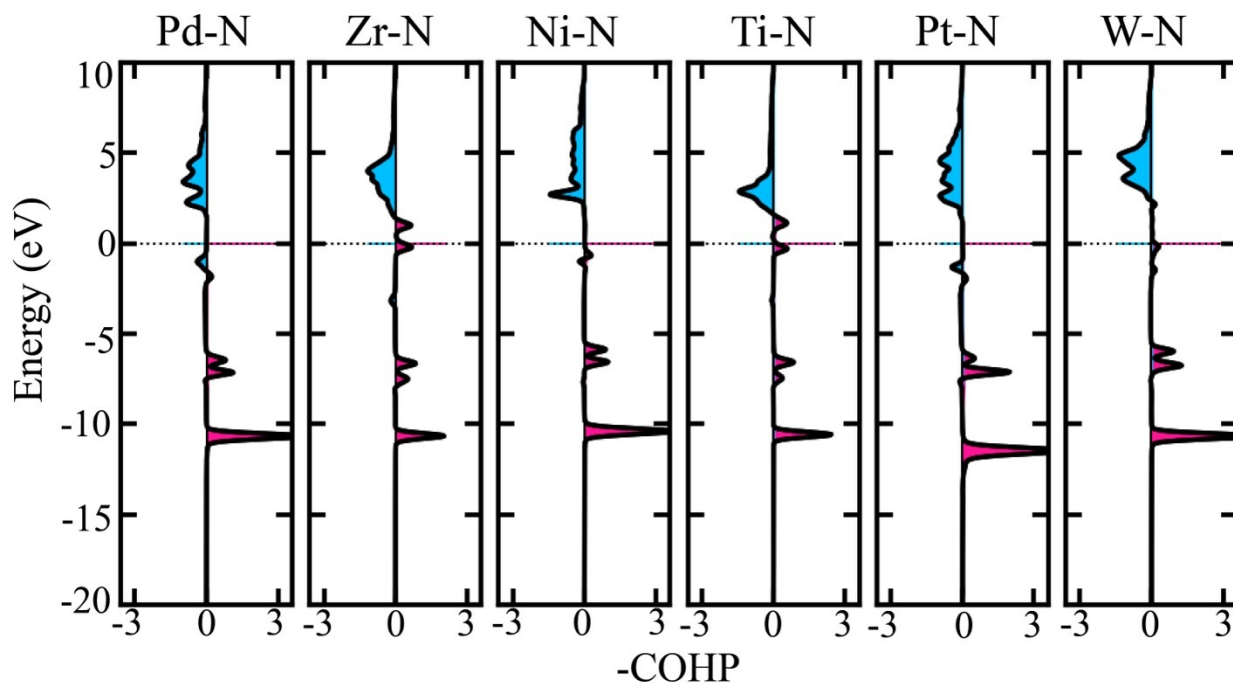


**Fig. S6** COHP analysis of *transition metal-nitrogen (TM-N)* bond for N<sub>2</sub> molecule bound to Pd (ZrO), Ni (TiO), and Pt (WC) supported on graphene where blue shaded regions represent antibonding states, and red shaded regions represent bonding states. Here, a negative COHP value (bonding region) suggests that there is bonding interaction between the TM and N. On the other hand, a positive COHP value (anti-bonding region) indicates anti-bonding interactions, typically weakening the bond. Strong p-d hybridization would manifest as a prominent bonding region in the negative COHP that can be attributed to both p (from nitrogen) and d (from TM) orbitals. To examine this interaction, we also focus on the energy region where the TM-N bond forms. For p-d hybridization, the key energy range is typically near the Fermi level or in the region where nitrogen's p orbitals overlap with the metal's d orbitals. Fig. S6 shows that negative COHP contribution around the energy range of the TM's d orbitals and N's p orbitals (see 0 eV set the Fermi level) for TM atoms of superatom; especially for Zr-N and Ti-N, this is a strong indication of p-d hybridization.

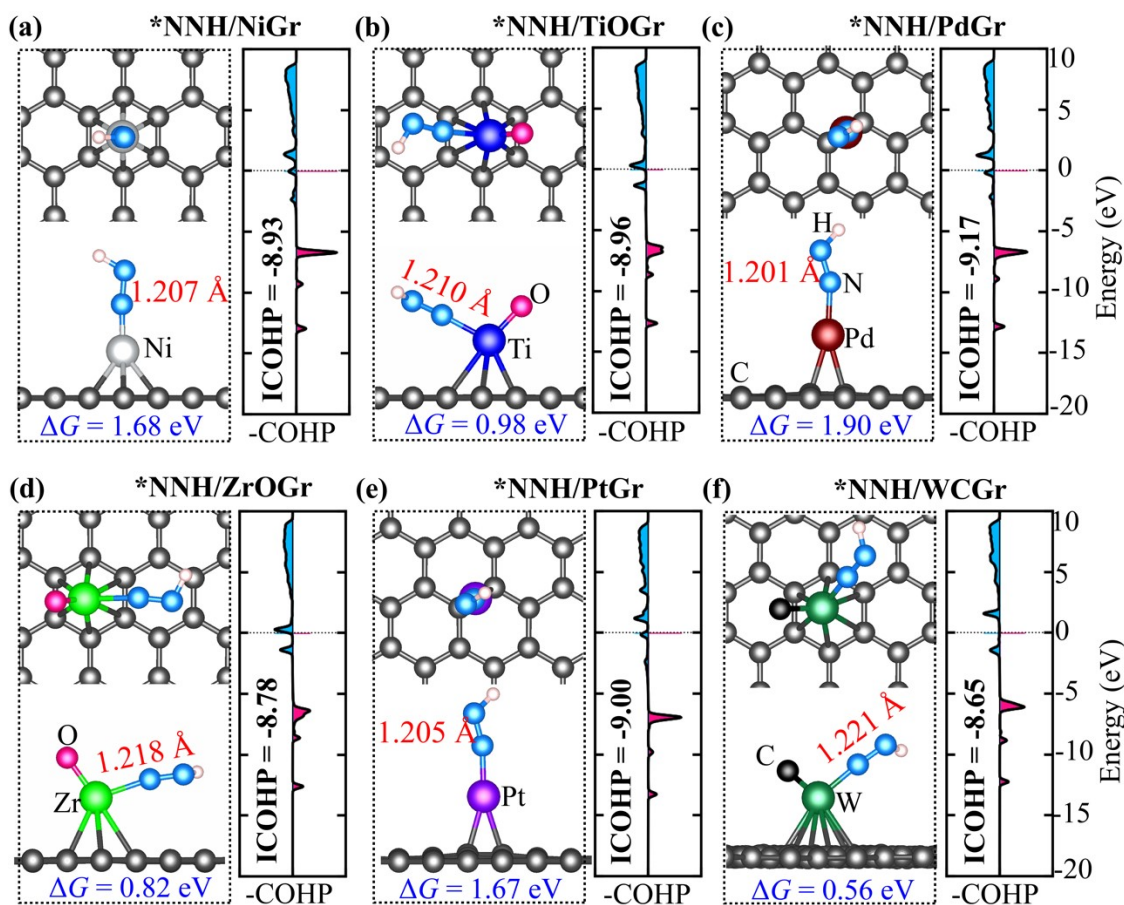


**Fig. S7** (Left) Top and side views of the most stable atomic configurations for the \*NNH intermediate on (a) Ni, (b) TiO, (c) Pd, (d) ZrO, (e) Pt, and (f) WC supported on graphene where the NN bond distances and the free energy changes are depicted. (Right) Crystal orbital Hamilton population (COHP) analysis for the NN bond, including the integrated COHP values (ICOHP), where antibonding and bonding states are illustrated in cyan and pink, respectively.

### Stability of Single Atoms and their Superatoms on Graphene

We initially employed the nudged elastic band (NEB) method to examine transition states. Since the single Pd atom is most stable at the bridge site on graphene, we explored three potential migration pathways: to the nearest bridge site (path 1), the second-nearest bridge site (path 2), and the third-nearest bridge site (path 3) (see Fig. S5 (a)). For path 1 and path 2, there is an intermediate top site between the initial state (IS) and final state (FS), while for path 3, there is an intermediate hollow site. The NEB results show that the top site serves as the transition state (TS) for all paths 1, path 2, and 3. Ultimately, all pathways converge to path 1, which has an energy barrier of 0.04

eV (Fig. S8 (b)). This low energy barrier suggests that a single Pd atom may not stay as a single atom on the graphene surface and will migrate and coalesce with other Pd atoms.

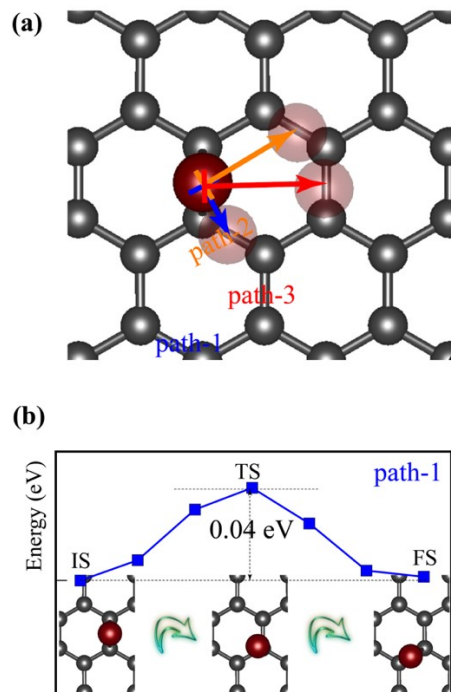


**Fig. S8** (a) Three potential pathways (path-1, path-2, path-3) for a Pd atom moving between bridge sites on a graphene surface. (b) The minimum energy path and the energy barrier between the initial state (IS) and the transition state (TS) for the Pd migration along the most favorable path (path-1).

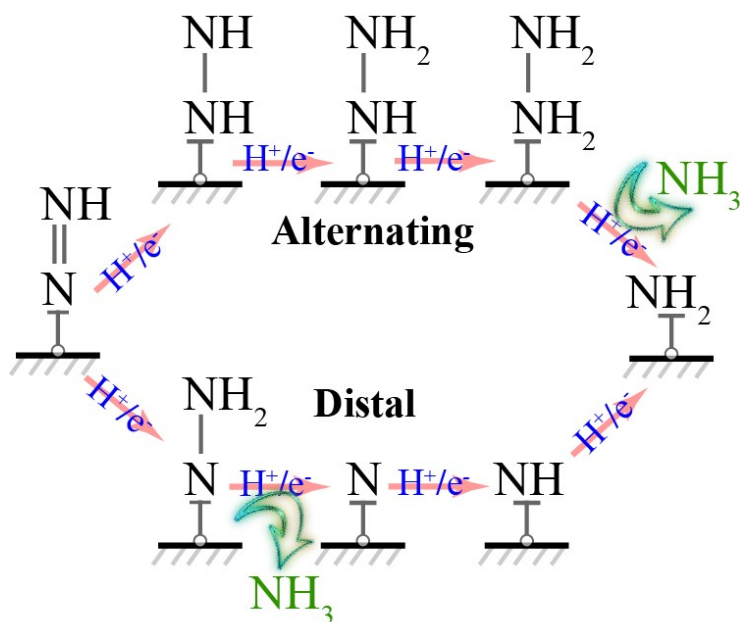


**Fig. S9.** Distal and Alternating pathways for NRR.

**Table S3.** Total energies ( $E_{\text{tot}}$ ), zero-point energies (ZPE), and entropy ( $S$ ) at  $T = 298.15$  K for  $^*\text{N}_2$ ,  $^*\text{NNH}$ ,  $^*\text{NHNH}$ ,  $^*\text{NHNH}_2$ ,  $^*\text{NH}_2\text{NH}_2$ ,  $^*\text{NH}$ ,  $^*\text{NH}_2$ ,  $^*\text{NH}_3$  intermediates.

	$E_{\text{total}}$ (eV)	ZPE (eV)	TS (eV)
$^*\text{N}_2$	-494.861	0.192	0.172
$^*\text{NNH}$	-497.766	0.468	0.175
$^*\text{NHNH}$	-502.042	0.764	0.191
$^*\text{NHNH}_2$	-505.981	1.131	0.212
$^*\text{NH}_2\text{NH}_2$	-508.971	1.468	0.215
$^*\text{NH}$	-489.830	0.337	0.051
$^*\text{NH}_2$	-495.102	0.664	0.133
$^*\text{NH}_3$	-498.237	1.004	0.215

#### References:

- 1 G. Kresse and J. Furthmüller, *Comput. Mater. Sci.*, 1996, 6, 15–50.
- 2 G. Kresse and D. Joubert, *Phys Rev B*, 1999, 59, 1758–1775.
- 3 M. J. Frisch, G. W. Trucks, H. B. Schlegel, G. E. Scuseria, M. A. Robb, J. R. Cheeseman, G. Scalmani, V. Barone, G. A. Petersson, H. Nakatsuji, X. Li, M. Caricato, A. V. Marenich, J. Bloino, B. G. Janesko, R. Gomperts, B. Mennucci, H. P. Hratchian, J. V. Ortiz, A. F. Izmaylov, J. L. Sonnenberg, D. Williams-Young, F. Ding, F. Lipparini, F. Egidi, J. Goings,

- B. Peng, A. Petrone, T. Henderson, D. Ranasinghe, V. G. Zakrzewski, J. Gao, N. Rega, G. Zheng, W. Liang, M. Hada, M. Ehara, K. Toyota, R. Fukuda, J. Hasegawa, M. Ishida, T. Nakajima, Y. Honda, O. Kitao, H. Nakai, T. Vreven, K. Throssell, J. A. Montgomery Jr., J. E. Peralta, F. Ogliaro, M. J. Bearpark, J. J. Heyd, E. N. Brothers, K. N. Kudin, V. N. Staroverov, T. A. Keith, R. Kobayashi, J. Normand, K. Raghavachari, A. P. Rendell, J. C. Burant, S. S. Iyengar, J. Tomasi, M. Cossi, J. M. Millam, M. Klene, C. Adamo, R. Cammi, J. W. Ochterski, R. L. Martin, K. Morokuma, O. Farkas, J. B. Foresman and D. J. Fox, Gaussian 16 Revision C.01. (2016).
- 4 P. E. Blöchl, *Phys. Rev. B*, 1994, 50, 17953–17979.
  - 5 J. P. Perdew, K. Burke and M. Ernzerhof, *Phys. Rev. Lett.*, 1996, 77, 3865–3868.
  - 6 S. Grimme, J. Antony, S. Ehrlich and H. Krieg, *J. Chem. Phys.*, DOI:10.1063/1.3382344.
  - 7 G. Henkelman, B. P. Uberuaga and H. Jónsson, *J. Chem. Phys.*, 2000, 113, 9901–9904.
  - 8 E. Skúlason, T. Bligaard, S. Gudmundsdóttir, F. Studt, J. Rossmeisl, F. Abild-Pedersen, T. Vegge, H. Jónsson and J. K. Nørskov, *Phys. Chem. Chem. Phys.*, 2012, 14, 1235–1245.
  - 9 A. A. Peterson and J. K. Nørskov, *J. Phys. Chem. Lett.*, 2012, 3, 251–258.
  - 10 A. D. Becke, *J. Chem. Phys.*, 1993, 98, 5648–5652.
  - 11 C. Lee, W. Yang and R. G. Parr, *Phys. Rev B*, 1988, 37, 785–789.
  - 12 P. J. Hay and W. R. Wadt, *J. Chem. Phys.*, 1985, 82, 270–283.